Tuning of graphene nanoribbon Landau levels by a nanotube

2009 J. Phys.: Condens. Matter 21 435302

(http://iopscience.iop.org/0953-8984/21/43/435302)

J. Phys.: Condens. Matter **21** (2009) 435302 (6pp) doi:10.1088/0953-8984/21/43/435302

Tuning of graphene nanoribbon Landau levels by a nanotube

T S Li[1], M F Lin[2] and S C Chang[1]

[1] Department of Electrical Engineering, Kun Shan University, Tainan, Taiwan, Republic of China
[2] Department of Physics, National Cheng Kung University, Tainan, Taiwan, Republic of China

E-mail: tsli@mail.ksu.edu.tw and mflin@mail.ncku.edu.tw

Received 3 July 2009, in final form 5 September 2009
Published 9 October 2009
Online at stacks.iop.org/JPhysCM/21/435302

Abstract

We investigate theoretically the effects of a nanotube on the graphene nanoribbon Landau level spectrum utilizing the tight-binding model. The addition of a nanotube changes the original dispersionless Landau subbands into distorted parabolic ones, creates additional band-edge states, and modifies the subband spacings. Moreover, the dispersion relations rely sensitively on the nanotube location. The nanotube–ribbon couplings disrupt the Landau wavefunctions and lift their spatial symmetry, which will change the selection rule of optical transitions. The numbers, frequencies and heights of the density of states (DOS) peaks are found to be strongly dependent on the magnetic flux density and the nanotube location. The evolution of the DOS peak with the magnetic flux density is explored. The graphene nanoribbon Landau levels are shown to be modified in an unexpected fashion by the nanotube–ribbon interactions. These predictions can be validated by measuring the spectra of scanning tunneling experiments or magneto-optical experiments, and they are most observable by placing the nanotube at the electron wavefunction localization sites.

(Some figures in this article are in colour only in the electronic version)

1. Introduction

Graphene is a flat monolayer of carbon atoms arranged in a two-dimensional (2D) honeycomb lattice. The recent realization of stable few-layer, including single-layer, graphenes has aroused considerable interest in the study of their electronic properties [1–8]. There are reports of unconventional electric field effects on the Hall coefficient [1], and a novel quantum Hall effect in monolayer [7] and bilayer graphenes [8]. These unusual electronic properties are due to the linear dispersion relations near the Dirac point. The carriers in graphene are massless Dirac fermions leading to shifted Hall plateaus [3, 7]. When graphene is patterned into a narrow ribbon, a graphene nanoribbon (GNR) will then be obtained. Just like carbon nanotubes (CNs), graphene nanoribbons are also 1D systems. They can be realized either by cutting mechanically exfoliated graphenes [7], or by patterning graphenes with lithographic techniques [2, 9]. In zigzag nanoribbons, there are strongly localized states at the zigzag edges, called 'edge states', which give rise to the partial flat bands in the range of $2\pi/3\sqrt{3}b \leqslant k \leqslant \pi/\sqrt{3}b$ [10]. $b = 1.42$ Å is the C–C bond length. At $k = \pi/\sqrt{3}b$, the electron wavefunction is perfectly localized at the zigzag edge. When k deviates from $\pi/\sqrt{3}b$, the wavefunction gradually penetrates and decays exponentially towards the inner sites. On the other hand, carbon nanotubes are rolled-up graphene sheets in cylindrical form, and their electronic properties are crucially dependent on the diameters and chiralities [11, 12]. Only armchair nanotubes are metallic and have linear subbands intersecting at the Fermi level. There are published reports about the magnetoelectronic properties of nanotubes [13–15].

When a perpendicular magnetic field is applied to a 2D graphene, it will confine the electron motion and leads to the Landau levels [16], which follow a simple relation $|E_{n_h}| = (\hbar v_F/l_B)\sqrt{2n_h}$, where v_F is the Fermi velocity and $l_B = \sqrt{\hbar/eB}$ is the magnetic length. A typical value is $l_B \approx 51.3$ Å for $B = 25$ T. The index $h = c$ or v represents the unoccupied conduction or occupied valence band, respectively. Recently, there are direct observations of Landau levels at graphite surfaces by scanning tunneling spectroscopy (STS) [17–19] and magnetotransmission measurements [20, 21]. Although l_B

sets the length scale of the lowest state wavefunction, higher state ones spread farther. For graphene nanoribbons in a perpendicular magnetic field, the electron motion is confined by both the magnetic potential and the ribbon boundary. In the limit of a strong magnetic field, $l_B \propto B^{-1/2} \to 0$. The electrons are confined mainly by the former. Their properties are independent of the latter, and reproduce the Landau levels of 2D graphene. This holds until the electron wavefunction touches the edge. In the actual situation, l_B is not infinitesimally small. Electrons deep inside the ribbon execute cyclotron orbits, and the orbits are interrupted by the edge when they are near the boundary. There exists competition between the magnetic confinement effect and the quantum confinement effect [22]. The insertion of a carbon nanotube will further alter the electronic properties by the nanotube–ribbon interactions. It is of interest to study how such interactions influence the Landau levels. In our previous work, the electronic properties of nanotube–ribbon hybrids made up of a single-walled carbon nanotube and a graphene nanoribbon are investigated by using the tight-binding method [23]. In comparison with recent local density approximation calculation results, excluding the bandgap opening for very narrow zigzag GNRs, the electronic structure of GNRs can still be quantitatively described by tight-binding calculations.

2. Theory

In this study, we consider an (m, m) armchair nanotube lying above a zigzag graphene nanoribbon with width N_w, which denotes the number of zigzag lines in the ribbon. There are $4m + 2N_w$ carbon atoms in the primitive unit cell. A schematic plot of a nanotube–ribbon hybrid system made up of a (6, 6) nanotube and an $N_w = 200$ zigzag nanoribbon is depicted in figure 1. The location of the nanotube is specified by x_{loc}, the ribbon zigzag line that is directly underneath the nanotube axis. The first Brillouin zone is confined within $|k| \leqslant \pi/\sqrt{3}b$. The nanotube and the ribbon are regarded as different subsystems. The Hamiltonian operator can be written as

$$\hat{\mathcal{H}}_{ij} = \begin{cases} t_{i,j} c_i^+ c_j & \text{for intra-subsystem hopping,} \\ W t_{i,j} e^{(d_{opt} - d_{ij})/\delta} c_i^+ c_j & \text{for inter-subsystem hopping,} \end{cases} \quad (1)$$

where $i = 1, 2, \ldots, 4m + 2N_w$. In equation (1), $t_{i,j}$ is the transfer integral. Only hoppings between the nearest neighbors are considered. The $2p_z$ orbitals are generally not parallel to each other, so the π bonding $V_{pp\pi}$ (=−2.66 eV = $-\gamma_0$) and σ bonding $V_{pp\sigma}$ (=6.38 eV) need to be considered in the inter-subsystem hoppings and the intra-nanotube hoppings. The nanotube–ribbon interactions are assumed to decay exponentially with interatom distance d_{ij} according to the model by Ahn *et al* [24]. $\delta = 0.45$ Å and the parameter W is chosen to be 1/8. c_i^+ and c_j are the creation and annihilation operators at sites i and j, respectively. The Lennard-Jones formula is employed to find the distance between the nanotube bottom and the ribbon plane, d_{opt} [25], at which the van der Waals potential between the nanotube and the ribbon is minimal. In the presence of a uniform magnetic field, the phase of the electron wavefunction determined by the vector potential will be modified. The magnetic field is along the z-axis. With the Landau gauge, the vector potential $\mathbf{A}$ is $(-By, 0, 0)$, which will induce an extra phase factor $\exp(i2\pi \Delta G_{\mathbf{R}}/\phi_0)$ in the Hamiltonian matrix element between sites i and j. $\Delta G_{\mathbf{R}} = \int_{\mathbf{R}_i}^{\mathbf{R}_j} \mathbf{A} \cdot d\vec{l}$ and $\phi_0 = 2\pi\hbar/e$ is the magnetic flux quantum. The dangling bonds on the edge sites are assumed to be terminated by hydrogen atoms, and they will not contribute to the electronic states near the Fermi level [11, 22]. After diagonalizing the Hamiltonian, the state energy $E^{c,v}(B)$ can be obtained. The superscripts c and v represent the conduction and the valence bands, respectively.

3. Results and discussion

We have computed the energy dispersions of zigzag graphene nanoribbons $N_w = 200$, corresponding to an actual ribbon width of 424.6 Å. At $B = 0$, there are parabolic bands and partial flat bands at $E_F = 0$ (not shown). Most of the subbands are parabolic. The partial flat bands are caused by the localized edge states [10, 22, 26]. At $B = 25$ T, the original parabolic bands become combinations of the parabolic bands and the developing Landau subbands with shifted energies (figure 1(b)). The Landau subbands are dispersionless in the vicinity of $k = 2\pi/3\sqrt{3}b$. Not only the dispersionless k-range but also the number of the Landau subbands grows with N_w. It is worth mentioning that the Landau level energies are independent of N_w when the ribbon is sufficiently wide. In such a case, l_B is much smaller than the ribbon width, and the low-energy electrons are confined mainly by the magnetic potential. Their properties are independent of the ribbon boundary. The Landau level spacings rise with growing B. The number of discrete levels decreases but the state degeneracy at each level increases with incrementing B. That is to say, the total number of electron states is conserved, and the states condense into Landau levels. Finally, the energy bands are symmetric about the Fermi level. The addition of a nanotube alters the band structures considerably. The original dispersionless Landau levels at $B = 25$ T are changed into distorted parabolic subbands. The nanotube–ribbon couplings modify the subband curvature, create additional band-edge states, and change the subband spacing, and the energy bands are no longer symmetric about $E_F = 0$ (figures 1(c) and (d)). Such energy band distortion varies with x_{loc}, and is most significant when the nanotube is situated at the electron wavefunction localization sites. On the other hand, higher-energy subbands are almost unaffected by the nanotube. They closely resemble the corresponding subbands of GNR at $B = 0$. This indicates that the electronic properties of the higher-energy subbands are dominated by the quantum confinement effect, and the magnetic field or the addition of a nanotube has little influence on them. The (6, 6) armchair nanotube originally has linear subbands intersecting at the Fermi level. The nanotube–ribbon interactions mix these linear dispersions with the GNR subbands, and change them into distorted parabolic subbands.

The characteristics of the wavefunctions are investigated. The envelope function Ψ_{n_c} of GNR can be decomposed into four subenvelope functions: $\Psi_{n_c} = \Psi_{n_c}(A^o) + \Psi_{n_c}(A^e) +$

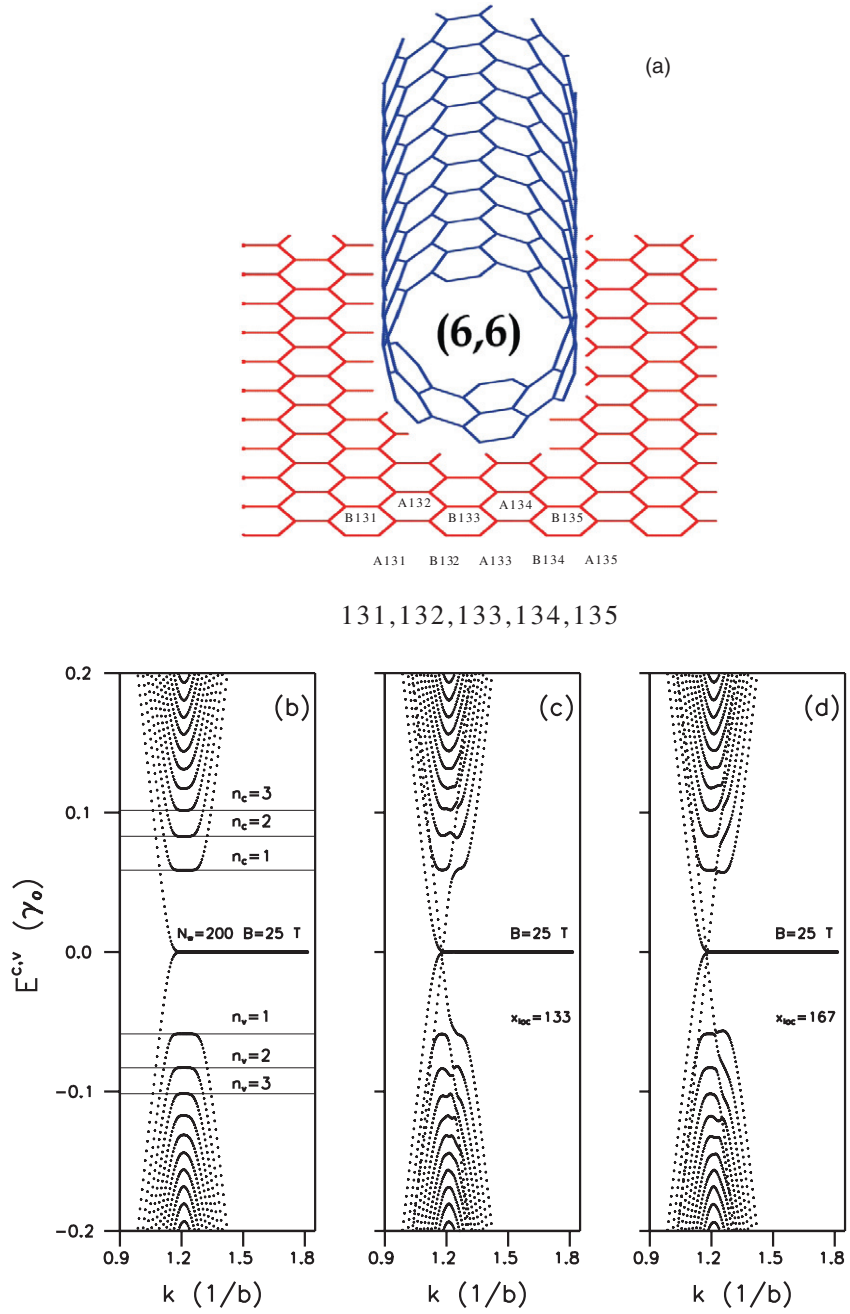

Figure 1. (a) Schematic plot of a nanotube–ribbon hybrid made up of a (6, 6) carbon nanotube and an $N_w = 200$ zigzag graphene nanoribbon with $x_{loc} = 133$. (b) The low-energy subbands of $N_w = 200$ graphene nanoribbons at $B = 25$ T. The low-energy subbands of nanotube–ribbon hybrid ((6, 6) CN and $N_w = 200$ GNR) at (c) $x_{loc} = 133$ and (d) $x_{loc} = 167$, with $B = 25$ T.

$\Psi_{n_c}(B^o) + \Psi_{n_c}(B^e)$ [26], where A^o, A^e, B^o, and B^e represent A or B atoms at the odd or even zigzag lines of the GNR. At $B = 0$, $\Psi_{n_c=0}(A^o)$, $\Psi_{n_c=0}(A^e)$, $\Psi_{n_c=0}(B^o)$ and $\Psi_{n_c=0}(B^e)$ are the localized edge states, which are strongly confined at one of the zigzag edge. The Ψ_{n_c} with $n_c \geqslant 1$ are the square well wavefunctions. When $B \neq 0$, $\Psi_{n_c=0}(A^o)$ and $\Psi_{n_c=0}(A^e)$ are only slightly influenced (dashed curves in figures 2(a) and (b)), and they are still the localized edge states, while $\Psi_{n_c=0}(B^o)$ and $\Psi_{n_c=0}(B^e)$ change to Landau wavefunctions. The geometry is left–right symmetrical, and the distinction between A and B sites is entirely due to the gauge chosen for the vector potential. The quantum mode is determined by the B-site Landau wavefunction. At $k = 2\pi/3\sqrt{3}b$, $\Psi_{n_c=0}(B^o)$, $\Psi_{n_c=0}(B^e)$, $\Psi_{n_c=1}(A^o)$ and $\Psi_{n_c=1}(A^e)$ have zero node and are the Gaussian function localized at the ribbon center. $\Psi_{n_c=1}(B^o)$, $\Psi_{n_c=1}(B^e)$, $\Psi_{n_c=2}(A^o)$ and $\Psi_{n_c=2}(A^e)$ have one node and distribute mainly at 1/3 and 2/3 of the ribbon (figure 2), corresponding to x_{loc} =67 and 133, respectively. The Landau wavefunctions Ψ_{n_c} of GNR with $n_c \geqslant 1$ at $k = 2\pi/3\sqrt{3}b$ are linear combinations of harmonic oscillator wavefunctions $\phi_{n_c-1}(A^o)$, $\phi_{n_c-1}(A^e)$, $\phi_{n_c}(B^o)$ and $\phi_{n_c}(B^e)$ [26], where ϕ_{n_c} is the product of the Hermite polynomial H_{n_c} and the Gaussian function. The parity of ϕ_{n_c} is even or odd when n_c is even or odd, respectively. n_c also denotes the number of nodes.

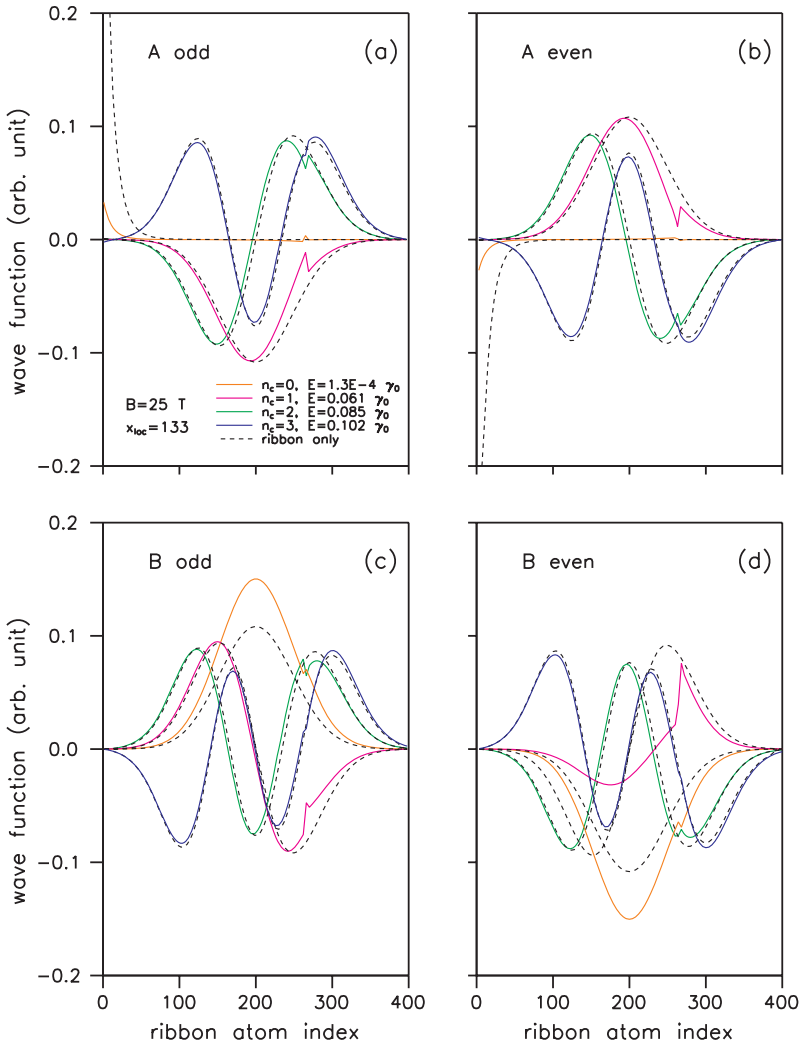

Figure 2. The envelope functions of the nanotube–ribbon hybrid at $k = 2\pi/3\sqrt{3}b$, $x_{\rm loc} = 133$ and $B = 25$ T on (a) A odd sites, (b) A even sites, (c) B odd sites and (d) B even sites of the ribbon.

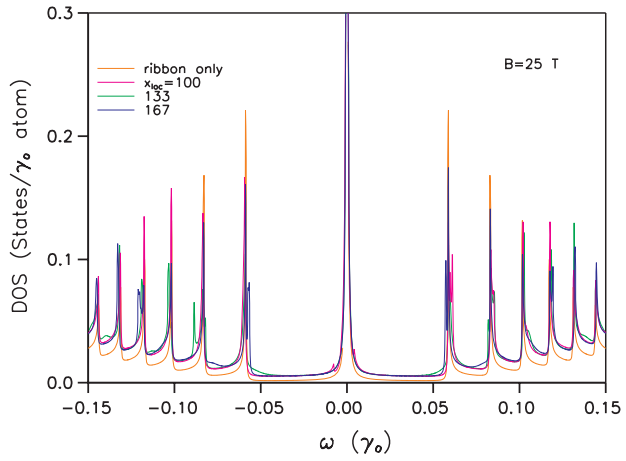

Figure 3. Density of states per atom of the $N_{\rm w} = 200$ graphene nanoribbon and nanotube–ribbon hybrid ((6, 6) CN and $N_{\rm w} = 200$ GNR) at $B = 25$ T and different $x_{\rm loc}$.

With the presence of the nanotube, there are significant changes in the low-energy ($n_{\rm c} = 0$, 1) wavefunctions, while the high-energy ($n_{\rm c} = 2$, 3) ones only modify slightly. The amplitudes of $\Psi_{n_{\rm c}=0}(\mathrm{A^o})$ and $\Psi_{n_{\rm c}=0}(\mathrm{A^e})$ decrease and those of $\Psi_{n_{\rm c}=0}(\mathrm{B^o})$ and $\Psi_{n_{\rm c}=0}(\mathrm{B^e})$ increase. The nanotube–ribbon interactions change the electron distribution between A and B atoms of the GNR, and cause electron transfer between GNR and CN atoms. For the $n_{\rm c} = 0$ state, there is electron migration from A to B atoms of the GNR, and there also exists electron transfer from CN to B atoms of the GNR. The GNR wavefunctions deviate from those of the harmonic oscillator, and such deviation varies with $x_{\rm loc}$ and $n_{\rm c}$. The nanotube–ribbon hoppings introduce kinks in the wavefunctions at $x_{\rm loc}$. The Landau wavefunctions of the valence bands also modified by the nanotube (not shown), and the modifications are similar to but not exactly the same as those of the conduction bands. The nanotube induced energy band distortions mentioned previously are most significant when the nanotube is placed at the positions where the GNR wavefunctions attain their peak values. Finally, the wavefunctions lose their spatial symmetry. The optical absorption spectrum is determined by the velocity matrix element $\langle \Psi^{\rm c}_{n_{\rm c}} | \hat{E} \cdot \vec{P}/m | \Psi^{\rm v}_{n_{\rm v}} \rangle$ [26]. The momentum operator $\vec{P}$ is the linear combination of the harmonic oscillator raising and lowering operators $a^\dagger$ and a. Considering the orthogonal properties of ϕ_{n_h}, the velocity matrix element of

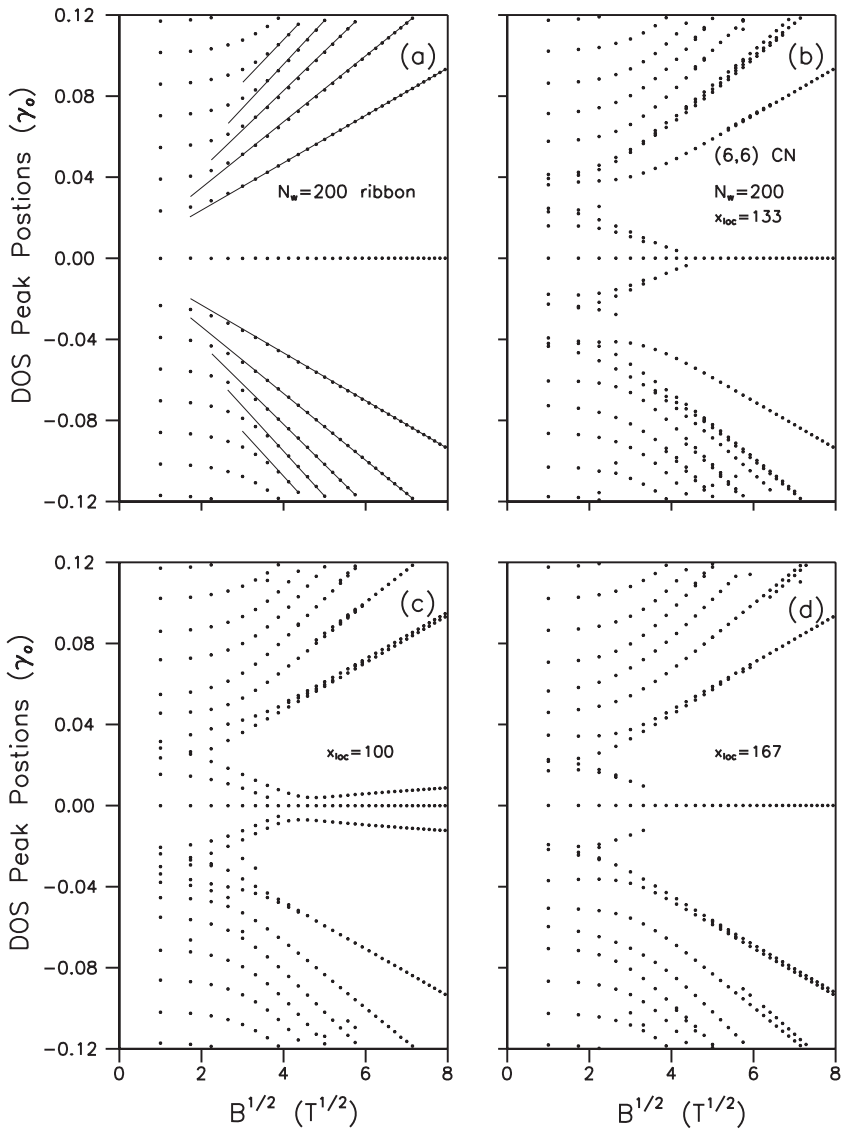

Figure 4. The dependence of the low-energy DOS peak positions on $\sqrt{B}$ for $N_w = 200$ graphene nanoribbon (a) and nanotube–ribbon hybrid with $x_{loc} = 100$ (b), $x_{loc} = 133$ (c), and $x_{loc} = 167$ (d). In (a), solid lines are drawn to guide the eyes.

the GNR can be derived as $C_1\delta_{n_c,n_v+1} + C_2\delta_{n_c,n_v-1}$ [26]. The selection rule is $n_v - n_c = \pm 1$ for Landau levels in the GNR. In the case of the nanotube–ribbon hybrid, this selection rule no longer holds. For example, the transition channel from $n_v = 1$ to $n_c = 1$ is forbidden in the GNR, but such transition is allowed in the nanotube–ribbon hybrid.

An important parameter to characterize the band structure is the density of states (DOS), which is defined as

$$D(\omega) = \sum_{c,v} \int_{1stBZ} \frac{dk}{(2\pi)^2} \frac{\Gamma}{(\omega - E^{c,v})^2 + \Gamma^2}, \qquad (2)$$

where $\Gamma = 2 \times 10^{-4}\ \gamma_0$ is the broadening parameter. In graphene nanoribbons, there are many 1D parabolic subbands. Consequently, DOS will exhibit many divergent peaks in the asymmetric square root form (the van Hove singularities). The peak energies correspond to the band-edge state energies (E_{ed}). The height of the peak is proportional to the inverse square root of the subband curvature (or the square root of the electron effective mass). When the subbands are concave downward and upward, the associating DOS would exhibit the divergent peak in the $1/\sqrt{\omega - E_{ed}}$ and $1/\sqrt{E_{ed} - \omega}$ form, respectively. There are prominent divergent peaks at E_F (figure 3), resulting from the partial flat bands. Neighboring low-energy DOS peaks will merge as B increases. The spacings between adjacent peaks rise with increasing B. The above-mentioned Landau level distortions are also reflected in the DOS. The addition of a nanotube creates many new band-edge states, and disrupts the DOS single peaks into multiple peaks. Such DOS peak disruption is more prominent in the low-energy regime. Finally, the DOS peak disruption also depends on x_{loc}. On the other hand, the DOS peak positions can be directly probed by the STS measurements [17–19], and they are also closely related to the absorption peaks in magnetotransmission experiments [20, 21]. Therefore, the evolution of the DOS peak positions with the magnetic flux density can be determined

experimentally, and deserves detailed investigations. For the graphene nanoribbon, they first obey the relation $E \propto B$ at small B. At large B, Landau levels appear, and the relation becomes $E \propto \sqrt{B}$ (figure 4(a)). The electron energies of 2D graphene in a perpendicular magnetic field exhibit the Landau levels [16], $|E_{n_h}| = (\hbar v_F/l_B)\sqrt{2n_h} = v_F\sqrt{2n_h\hbar eB}$. In the limit of a strong magnetic field, the electronic properties of the graphene nanoribbon are dominated by the magnetic field, and reproduce the Landau levels of 2D graphene. Therefore, the DOS peak positions of graphene nanoribbon vary with $\sqrt{B}$ at large B. At small B, there is no Landau level in the graphene nanoribbon, and the energy bands are parabolic. The corresponding DOS peak positions vary linearly with B. The nanotube–ribbon coupling modifies the low-energy band structure significantly and introduces new band-edge states which correspond to additional DOS peaks in figures 4(b)–(d). There are DOS peaks emerging near the Fermi level, and their positions decay with increasing B (figures 4(b)–(d)). Moreover, as the nanotube is placed at the ribbon center ($x_{loc} = 100$), DOS peak position curves drop initially and then rebound with rising B (figures 4(b)). These newly generated DOS peak behaviors deviate from the mentioned simple linear B to square root B dependence.

4. Concluding remarks

In conclusion, the effects of a nanotube on the graphene nanoribbon Landau levels are studied theoretically by the tight-binding model. For a graphene nanoribbon in a perpendicular magnetic field, there will be Landau levels when B is large. The addition of a nanotube changes the original dispersionless Landau subbands into distorted parabolic ones, creates additional band-edge states, and modifies the subband spacing. In addition, the dispersion relations are found to rely sensitively on the nanotube location. The nanotube–ribbon couplings disrupt the Landau wavefunctions and lift their spatial symmetry, which will change the selection rule of optical transitions. The nanotube–ribbon interactions cause electron transfer between A and B atoms of the GNR, and between the GNR and CN subsystems. The variations of the band structures will be directly reflected in the DOS. The numbers and frequencies of the DOS peaks are strongly dependent on the magnetic flux density and the nanotube location. The evolution of the DOS peak with the magnetic flux density is explored. The Landau levels are shown to be modified in an unexpected fashion by the nanotube–ribbon interactions. These predictions can be validated by measuring the spectra of STS or magneto-optical experiments, and they are most observable by placing the nanotube at the electron wavefunction localization sites.

Acknowledgment

This work was supported in part by the National Science Council of Taiwan, Republic of China, under grant No NSC 98-2112-M-168-001-MY2.

References

[1] Novoselov K S, Geim A K, Morozov S V, Jiang D, Zhang Y, Dubonos S V, Grigorieva I V and Firsov A A 2004 *Science* **306** 666
[2] Berger C, Song Z M, Li T B, Li X B, Ogbazghi A Y, Feng R, Dai Z T, Marchenkov A N, Conrad E H, First P N and de Heer W A 2004 *J. Phys. Chem.* B **108** 19912
[3] Novoselov K S, Geim A K, Morozov S V, Jiang D, Katsnelson M I, Grigorieva I V, Dubonos S V and Firsov A A 2005 *Nature* **438** 197
[4] Zhang Y, Small J P, Amori M E S and Kim P 2005 *Phys. Rev. Lett.* **94** 176803
[5] Bunch J S, Yaish Y, Brink M, Bolotin K and McEuen P L 2005 *Nano Lett.* **5** 2887
[6] Zhang Y, Small J P, Pontius W V and Kim P 2005 *Appl. Phys. Lett.* **86** 073104
[7] Zhang Y, Tan Y-W, Stormer H L and Kim P 2005 *Nature* **438** 201
[8] Novoselov K S, McCann E, Morozov S V, Falko V I, Katsnelson M I, Zeitler U, Jiang D, Schedin F and Geim A K 2006 *Nat. Phys.* **2** 177
[9] Berger C, Song Z M, Li X, Wu X, Brown N, Naud C, Mayou D, Li T, Hass J, Marchenkov A N, Conrad E H, First P N and de Heer W A 2006 *Science* **312** 1191
[10] Nakada K, Fujita M, Dresselhaus G and Dresselhaus M S 1996 *Phys. Rev.* B **54** 17954
[11] Hamada N, Sawada S and Oshiyama A 1992 *Phys. Rev. Lett.* **68** 1579
[12] Odom T W, Huang J L, Kim P and Lieber C M 1998 *Nature* **391** 62
[13] Ajiki H and Ando T 1993 *J. Phys. Soc. Japan* **62** 1255
[14] Lu J P 1995 *Phys. Rev. Lett.* **74** 1123
[15] Shyu F L, Chang C P, Chen R B and Lin M F 2003 *Phys. Rev.* B **67** 045405
[16] McClure J W 1956 *Phys. Rev.* **104** 666
[17] Morgenstern M, Klijn J, Meyer C and Wiesendanger R 2003 *Phys. Rev. Lett.* **90** 056804
[18] Matsui T, Kambara H, Niimi Y, Tagami K, Tsukada M and Fukuyama H 2005 *Phys. Rev. Lett.* **94** 226403
[19] Niimi Y, Kambara H, Matsui T, Yoshioka D and Fukuyama H 2006 *Phys. Rev. Lett.* **97** 236804
[20] Sadowsk M L, Martinez G and Potemski M 2006 *Phys. Rev. Lett.* **97** 266405
[21] Orlita M, Faugeras C, Martinez G, Maude D K, Sadowski M L and Potemski M 2008 *Phys. Rev. Lett.* **100** 136403
[22] Huang Y C, Chang C P and Lin M F 2007 *Nanotechnology* **18** 495401
[23] Li T S, Chang S C, Lien J Y and Lin M F 2008 *Nanotechnology* **19** 105703
[24] Ahn K H, Kim Y H, Wiersig J and Chang K J 2003 *Phys. Rev. Lett.* **90** 026601
[25] Girifalco L A and Lad R A 1956 *J. Chem. Phys.* **25** 693
[26] Huang Y C, Chang C P and Lin M F 2008 *J. Appl. Phys.* **103** 073709